

## Observational aspects of a class of dark matter spacetimes

Ashok B. Joshi<sup>1,\*</sup>, Divya Tahelyani<sup>1,†</sup>, Dipanjan Dey<sup>2,‡</sup> and Pankaj S. Joshi<sup>3,1,§</sup>

<sup>1</sup>*International Center for Cosmology, Charusat University, Anand, Gujarat 388421, India*

<sup>2</sup>*Department of Mathematics and Statistics, Dalhousie University, Halifax, Nova Scotia, B3H 3J5, Canada*

<sup>3</sup>*Cosmology Centre, Ahmedabad University, Ahmedabad, Gujarat 380009, India*



(Received 14 December 2022; accepted 23 October 2023; published 14 November 2023)

Various astrophysical and cosmological observations today serve as indirect evidence of the existence of dark matter in the Universe. In the present work, we propose a class of spacetimes that show some important characteristics relevant to the spacetime of a dark matter halo. These spacetimes are static and spherically symmetric solutions of the Einstein field equations. The proposed spacetimes satisfy the flat velocity profile of a galactic object far away from the center, they give good agreement to the astrometric data of the S2 star, and these also cast a central shadow. Using the Penrose diagram, we show that the causal nature of the central singularity here is null. This single spacetime model for galactic dark matter may therefore be used to explain some of the properties of galactic dynamics at different length scales.

DOI: [10.1103/PhysRevD.108.104034](https://doi.org/10.1103/PhysRevD.108.104034)

### I. INTRODUCTION

One source of indirect evidence for the existence of dark matter comes from observations of the rotation curves of galaxies. The rotation curves of the spiral galaxies demonstrate that the velocity of the stars and gas in the outer regions of these galaxies becomes almost constant [1]. Therefore, their rotation curves are flat, in contrast to what is expected from Newtonian dynamics. The most general explanation is the presence of an additional, unseen mass component that causes the observed motion. The galactic rotation curves are generally divided into three parts: a bulge, a disk, and a dark halo. In general, the matter distribution in our Galaxy is classified into four different parts. The radial distance from  $10^{-4}$  to 2 pc consists of young stars that follow Keplerian law ( $v \propto r^{-1/2}$ ) [2]. Noncircular motions of young stars have frequently been observed near the Galactic Center. An intermediate spheroidal bulge structure comprises older stars that follow the exponential spheroidal model and ranges from 2 to  $10^3$  pc. The region  $10^3$ – $10^4$  pc is called an extended flat disk in which dust and gas are present, which is a star-formation zone. The region  $10^4$ – $10^5$  pc is dominated by dark matter called a spherical or outer halo [2].

The nature of dark matter remains very much unknown as of now. There are many possible candidates for dark matter, such as heavy neutrinos, weakly interacting massive particles, micro- and primordial black holes, etc. [3], and

others. As an alternative to dark matter, several theoretical models, based on a modification of Newton's law or of general relativity, have been proposed so far to explain the behavior of the Galactic rotation curves [4–12]. Until now, there has been no complete theory that predicts the direct detection of dark matter. Our Milky Way Galaxy serves as an experimental hub to test general relativity on the largest as well as the smallest scale. Sagittarius A\* (Sgr A\*) is a massive and compact radio source located at the center of our Galaxy. One of the primary concerns about Sgr A\* is its true identity. It is still a mystery whether it is a black hole or an alternative, such as a naked singularity, a wormhole, or any other exotic compact object. Many investigations into gravitational collapse have been conducted, and it has been discovered that the final state of collapse is not necessarily a black hole. There is a considerable amount of research showing that null- and timelike singularities can be formed during the gravitational collapse of physically plausible matter clouds [13–17], which contradicts the cosmic censorship conjecture proposed by Penrose [18]. The Galactic Center with a strong gravity region can be explored by investigating numerous observable factors, such as the shadow of the ultracompact object, the relativistic orbit of the S2 star, and accretion disk features, etc. In 2019, the Event Horizon Telescope (EHT) released the first groundbreaking horizon-scale image for M87 [19], a supermassive compact object present at the center of galaxy Messier 87. This was followed by the recent release of the first image of Sgr A\* [20–28]. To know the actual theoretical framework of the geometry around the Sgr A\* compact object, many groups are working on the shadow and accretion disk properties of the compact object [29–46]. On the other hand, decades of continuous

\*gen.rel.joshi@gmail.com

†tahelyanidivya118@gmail.com

‡deydipanjan7@gmail.com

§psjcosmos@gmail.com

astrometric and spectroscopic observations by GRAVITY, SINFONI, and the UCLA Galactic Center group provide useful information about the central compact object by using the trajectories of “S” stars. These S stars are located very close to the Galactic Center and are orbiting around Sgr-A\* with a very high velocity [47–50]. In this context, there is a large amount of literature in which the nature of the timelike trajectories and orbital precession of a test particle in various spacetime geometries is extensively studied [51–69].

In [70], Nampalliwar *et al.* derived the spacetime metric around a Schwarzschild black hole (BH) in between the range  $r_b - R_{sp}$  by assuming the power-law density profile given by Nishikawa *et al.* [71]. By using the observational data, the metric is tested where the best-fit value of  $r_b$  and  $R_{sp}$  are around  $9.4M_{\text{BH}}$  and 0.91 kpc, respectively. In the  $r < r_b$  radius, the usual Schwarzschild metric is present and the  $r > R_{sp}$  metric can be matched with either the Burkert-Salucci profile [72,73] or the Navarro-Frenk-White (NFW) profile [74]. In our paper, we investigate a distribution of dark matter in the range  $0 < r < R_b$ . In the  $r < R_b$ , the Newtonian metric (a weak gravitational field region of the Schwarzschild metric) is present.

In the present work, we propose a new procedure to model the spacetime of a galactic dark matter halo in the framework of general relativity. We construct a class of spacetimes here that can model the flat rotation curves far from the center, and these have a photon sphere near the center. First, we use the well-established observational constancy of the rotation curves far away from the galactic center. Further, we use the conditions for the presence of a photon sphere in spacetime. These properties allow us to obtain the metric components for the spacetime we construct here. The available observational data of the astrometric positions of the S2 star (one of the stars in the S-stars family) can provide useful constraints on the proposed model. We obtain the timelike orbit of the massive particle in the proposed dark matter spacetime and constrain the free parameters of the metric by fitting the theoretical orbit with the observational data of the S2 star orbit. Furthermore, we study the rotation curve, redshift, and shadow properties using the best-fitted parameters.

The paper is organized as follows: In Sec. II, we construct the class of spacetimes using the properties of the flat velocity curve and photon sphere. We also discuss the energy conditions and causal structure of spacetime in that section. Subsequently, in Sec. III, we study the particle trajectory in the proposed dark matter spacetime, and after that, we obtain the best-fitted parameter values using the orbital motion of the S2 star. Next, in Secs. IV and V, we study the circular velocity profiles far away from the center and the shadow properties of the spacetime using the best-fitted values of parameters. Finally, in Sec. VII, we conclude our results.

## II. CONSTRUCTION OF DARK MATTER SPACETIME

Observations show that almost 90% of the Galaxy should be made up of dark matter. Therefore, at a considerable distance from the center, we can assume that compared to dark matter, baryonic matter does not contribute significantly to the total energy density of the halo and hence to the dynamics of particles in the Galaxy. Therefore, after a certain distance, we can assume that the luminous matter acts as a test fluid that travels in the curvature created by the dark matter.

To begin with, we assume that stars behave as test particles that follow the timelike geodesics of a static and spherically symmetric spacetime. In this situation, the most generic form of the line element of spacetime is as follows:

$$ds^2 = -g_{tt}c^2dt^2 + g_{rr}dr^2 + r^2(d\theta^2 + \sin^2\theta d\phi^2), \quad (1)$$

where  $g_{tt}$ ,  $g_{rr}$  are the functions of  $r$  only, and the azimuthal part of the spacetime exhibits the spherical symmetry. In this section, we intend to derive a spacetime metric that possesses two properties: (i) a flat velocity curve away from the Galactic Center and (ii) a photon sphere near the Galactic Center.

The rotation curves of spiral galaxies are one of the most important indirect evidence of the existence of dark matter. In the spiral arms of these galaxies, neutral hydrogen (HI) clouds host millions of stars. The frequency shifts in these clouds’ 21 cm HI emission are used to measure the velocities of the stars that are hosted by the cloud. It is an empirical fact that, far from the Galactic Center, the celestial bodies follow almost circular orbits and the circular velocity of stars is a frame-dependent quantity. The shift in 21 cm HI emission occurs due to the Doppler effect caused by local Lorentzian motion of the stars. Therefore, to investigate the possible metric components that admit a flat velocity profile far away from the center, one needs to use the expression of the circular velocity of a particle measured by a stationary Lorentzian observer at one location in the orbit. The Lagrangian for the test particle traveling in any spacetime can be written as

$$2\mathcal{L} = g_{\mu\nu} \frac{dx^\mu}{ds} \frac{dx^\nu}{ds}, \quad (2)$$

where  $s$  is the affine parameter along the geodesic. For timelike geodesics, the affine parameter is the same as the proper time  $\tau$  of the particle. For the sake of simplicity, we constrain our analysis to the equatorial plane ( $\theta = \pi/2$ ). For the line element described in Eq. (1), it follows that

$$\begin{aligned} 2\mathcal{L} &= -g_{tt}\dot{t}^2 + g_{rr}\dot{r}^2 + r^2\dot{\theta}^2 + r^2\sin^2\theta\dot{\phi}^2 \\ &= \epsilon. \end{aligned} \quad (3)$$

Here, the dot indicates the derivative with respect to the proper time  $\tau$ . The null- and timelike geodesics are characterized by  $\epsilon = 0$  and  $\epsilon = -c^2$ , respectively. The conserved quantities, energy ( $e$ ) and angular momentum ( $h$ ), of the particle per unit rest mass can be obtained as follows:

$$-e = \frac{\partial \mathcal{L}}{\partial \dot{t}} = -g_{tt} c^2 \dot{t}, \quad (4)$$

$$h = \frac{\partial \mathcal{L}}{\partial \dot{\phi}} = r^2 \dot{\phi}. \quad (5)$$

Since for the timelike case  $2\mathcal{L} = -c^2$ , eliminating  $\dot{t}$  and  $\dot{\phi}$  using Eqs. (4) and (5), we obtain

$$E = e^2 c^2 = g_{tt} g_{rr} \dot{r}^2 + V_{\text{eff}}, \quad (6)$$

and the effective potential

$$V_{\text{eff}}(r) = g_{tt} \left( c^2 + \frac{h^2}{r^2} \right). \quad (7)$$

Here,  $E$  is the total energy of the particle. Since we are interested in the stable circular orbit of the test particle, the following conditions must be satisfied:

$$(a) \quad \dot{r} = 0 \quad (\text{circular orbit}), \quad (8)$$

$$(b) \quad \frac{dV_{\text{eff}}(r)}{dr} = 0 \quad (\text{extremum motion}), \quad (9)$$

$$(c) \quad \left. \frac{d^2 V_{\text{eff}}(r)}{dr^2} \right|_{\text{extrem}} > 0 \quad (\text{stable orbit}). \quad (10)$$

Solving the conditions (a) and (b) for  $e$  and  $h$ , we obtain

$$e = \sqrt{\frac{2g_{tt}^2}{2g_{tt} - rg'_{tt}}}, \quad (11)$$

$$h = c \sqrt{\frac{r^3 g'_{tt}}{2g_{tt} - rg'_{tt}}}, \quad (12)$$

where  $(\prime)$  denotes derivative with respect to the radial coordinate  $r$ . By substituting the above expressions of  $e$  and  $h$  in Eqs. (4) and (5), the four-velocity of the particle becomes

$$u^t = \dot{t} = \frac{1}{c^2} \sqrt{\frac{2}{2g_{tt} - rg'_{tt}}}, \quad u^\phi = \dot{\phi} = c \sqrt{\frac{g'_{tt}}{r(2g_{tt} - rg'_{tt})}}. \quad (13)$$

While moving along orbit, when the position of the particle coincides with the position of the observer, the velocity of the particle can be measured at that instant of time by using

the local Lorentz tetrad frame of the observer. The basis vectors of the orthonormal tetrad frame of the stationary observer can be written as [75]

$$e_i^\alpha = \left\{ \frac{1}{\sqrt{c^2 g_{tt}}}, 0, 0, 0 \right\}, \quad (14)$$

$$e_{\hat{r}}^\alpha = \left\{ 0, \frac{1}{\sqrt{g_{rr}}}, 0, 0 \right\}, \quad (15)$$

$$e_{\hat{\theta}}^\alpha = \left\{ 0, 0, \frac{1}{r}, 0 \right\}, \quad (16)$$

$$e_{\hat{\phi}}^\alpha = \left\{ 0, 0, 0, \frac{1}{r \sin \theta} \right\}, \quad (17)$$

where  $(\hat{\cdot})$  corresponds to the coordinates of the orthonormal tetrad frame. Using the above basis vectors, the  $t$  and  $\phi$  components of the four velocities in the observer's local frame can be obtained,

$$u^{\hat{t}} = \frac{1}{c^2} \sqrt{\frac{2g_{tt}}{2g_{tt} - rg'_{tt}}}, \quad u^{\hat{\phi}} = c \sqrt{\frac{rg'_{tt}}{2g_{tt} - rg'_{tt}}}. \quad (18)$$

The tangential velocity ( $v$ ) of the particle in the circular orbit as measured by the Lorentzian observer can be defined as

$$v = v^{\hat{\phi}} = \frac{u^{\hat{\phi}}}{u^{\hat{t}}} = c \sqrt{\frac{rg'_{tt}(r)}{2g_{tt}(r)}}. \quad (19)$$

We know that the observations in the spiral galaxy suggest that very far from the galactic center,  $v \approx \text{constant}$  [76]. Using this condition, the integration of the above equation gives the functional form of the  $g_{tt}(r)$ , which we denote as  $g_{tt_1}(r)$ ,

$$g_{tt_1}(r) = e^{\left( \frac{2V_c^2}{c^2} \right) \ln \left( \frac{r}{R_c} \right)}, \quad (20)$$

where  $V_c$  is the constant velocity of the stars far away from the center and  $R_c$  is the constant of integration. The functional form [Eq. (20)] of  $g_{tt}$  is valid only in the region of the flat rotation curve. To find the condition on  $g_{tt}$  in the region close to the center, we use the aforementioned second property of the metric: the presence of a photon sphere. We know that the photon sphere corresponds to the unstable circular orbits of the photons, and its presence in spacetime requires the existence of a maximum of the effective potential ( $\mathcal{V}_{\text{eff}}$ ) of null geodesics. For the spacetime described in Eq. (1), in the equatorial plane ( $\theta = \pi/2$ ), the null geodesics satisfies the relation

$$\frac{1}{b^2} = \frac{g_{tt}g_{rr}}{l^2} \left( \frac{dr}{dl} \right)^2 + \mathcal{V}_{\text{eff}}, \quad (21)$$

where the effective potential

$$\mathcal{V}_{\text{eff}} = \frac{g_{tt}}{r^2}, \quad (22)$$

and the impact parameter  $b = \frac{l}{\varepsilon}$ , where  $\varepsilon$  and  $l$  are conserved energy and conserved angular momentum of the photon, respectively.

At photon sphere radius ( $r_{ph}$ ), one can write  $\mathcal{V}_{\text{eff}}(r_{ph}) = \frac{\varepsilon^2}{l^2}$ ,  $\mathcal{V}'_{\text{eff}}(r_{ph}) = 0$ , and  $\mathcal{V}''_{\text{eff}}(r_{ph}) < 0$ . In order to obtain the spacetime metric that possesses a photon sphere, we start by considering an ansatz for the effective potential, which has a maximum as follows:

$$\mathcal{V}_{\text{eff}} = \frac{1}{r^2} e^{p - \left(\frac{r}{r_*}\right)^n}, \quad (23)$$

where  $p$  and  $r_*$  are constants. Using the condition  $\mathcal{V}'_{\text{eff}}(r_{ph}) = 0$ , we can calculate the radius of a photon sphere as

$$r_{ph} = \left( \frac{2}{n} \right)^{-\frac{1}{n}} r_*. \quad (24)$$

Substituting the expression of  $r_*$  from the above equation in Eq. (23), the form of effective potential becomes

$$\mathcal{V}_{\text{eff}} = \frac{1}{r^2} e^{p - \frac{2}{n} \left( \frac{r_{ph}}{r} \right)^n}. \quad (25)$$

From Eq. (22), we can write the second form of  $g_{tt}(r)$  (i.e.,  $g_{tt_2}$ ),

$$g_{tt_2} = e^{p - \frac{2}{n} \left( \frac{r_{ph}}{r} \right)^n}. \quad (26)$$

For the above type of form of  $g_{tt}$ , the maxima and upper bound of the effective potential coincide, which allows the spacetime to cast a shadow [29,32]. The functional form of  $g_{tt}$  in Eq. (20) becomes dominant as one moves away from the center, accounting for the particle's constant velocity in the outer parts of the galaxy. On the other hand, Eq. (26) dominates over small distances from the center and creates the photon sphere near the center. Now, Eqs. (20) and (26) can be combined to obtain a single expression of  $g_{tt}$  that exhibits both properties: a presence of a photon sphere near the center as well as a flat velocity profile farther away from the center,

$$g_{tt}(r) = q * e^{\left( p - 2 \left( \frac{c^2 - V_c^2}{c^2 n} \right) \left( \frac{r_{ph}}{r} \right)^n \right) + \frac{2V_c^2}{c^2} \ln \left( \frac{r}{R_c} \right)}, \quad (27)$$

where  $q$  is a constant that can be determined from the boundary conditions. Here, Eqs. (20) and (26) are

combined in such a way that the photon sphere still remains at the same radius  $r = r_{ph}$  in the merged expression of  $g_{tt}$ . This spacetime of the galactic dark matter halo cannot be an asymptotically flat spacetime. It should be matched with any asymptotically flat spacetime at some timelike hypersurface.

In general relativity, for the smooth matching of two spacetimes at a timelike or spacelike hypersurface, two junction conditions must be fulfilled on the matching hypersurface [77]. The first condition requires that the induced metric ( $h_{ab}$ ) on both sides of the matching hypersurface must be identical, and the second condition states that the extrinsic curvature ( $K_{ab}$ ) of the internal and external spacetimes at the matching hypersurface should be the same. The extrinsic curvature can be written in terms of the covariant derivative of normal vectors on the hypersurface,

$$K_{ab} = e_a^\alpha e_b^\beta \nabla_\alpha \eta_\beta, \quad (28)$$

where  $e_a^\alpha$  is the tangent to the hypersurface and  $\eta^\beta$  is the normal to that hypersurface. We suppose that the spacetime geometry outside the halo is described by the Schwarzschild spacetime in the weak field limit, which joins with the internal dark matter geometry at the matching hypersurface  $r = R_b$ . The line element of exterior Schwarzschild spacetime in the weak field limit can be written as

$$ds_{\text{ext}}^2 = -c^2(1 - \alpha)dt^2 + (1 + \alpha)dr^2 + r^2 d\Omega^2, \quad (29)$$

where  $\alpha = \frac{2V_b^2}{c^2}$  and  $d\Omega^2 = d\theta^2 + \sin^2 \theta d\phi^2$ . Here,  $V_b$  is the velocity of the particle, which would be the same as the constant velocity of the stars in the flat velocity profile region. It should be noted that  $R_b \gg r_{ph}$ . One can check that the spacetime geometry comprising the internal and external metrics is not smooth at the junction hypersurface  $r = R_b$ . Therefore, there must be a thin shell of matter at the junction. Using the induced metrics matching at the junction, we get  $q = c^2$  and  $p = -\alpha$ . By considering the tangential velocity  $V_c = V_b$  at  $r = R_b$ , we can determine the integration constant  $R_c$  in Eq. (20). Thus, Eq. (20) becomes

$$g_{tt_1}(r) = e^{\left( \frac{2V_b^2}{c^2} \right) \ln \left( \frac{r}{R_b} \right)}. \quad (30)$$

The final temporal component of the internal metric  $g_{tt}(r)$  can be written as

$$g_{tt}(r) = c^2 \text{Exp} \left[ -\alpha - \frac{\beta(2 - \alpha)}{n} + \alpha \log \left( \frac{r}{R_b} \right) \right], \quad (31)$$

where  $\beta = \left( \frac{r_{ph}}{r} \right)^n$ .

We now address the question of how to obtain  $g_{rr}(r)$ . We proceed by solving Einstein's field equations to determine  $g_{rr}$  inside the halo. We consider that the dark matter that comprises the spherical halo is a fluid with the energy density  $c^2\rho(r)$ , radial pressure  $P_r(r)$ , and tangential pressures  $P_\theta(r)$  and  $P_\phi(r)$ . For the matching of the internal metric with the external Schwarzschild metric on the matching hypersurface, radial pressure at the matching boundary of the internal spacetime should be zero. For simplicity, we consider that the radial pressure inside the

internal spacetime is throughout zero. Now, one can solve Einstein's field equations with the condition  $T_1^1 = P_r = 0$  using previously determined  $g_{tt}(r)$  [Eq. (31)] and deduce the expression for  $g_{rr}(r)$  as

$$g_{rr}(r) = (1 + 2\beta + \alpha(1 - \beta)). \quad (32)$$

By substituting  $g_{tt}(r)$  and  $g_{rr}(r)$  in Eq. (1), the line element of the proposed dark matter spacetime becomes

$$ds_{\text{int}}^2 = -c^2 \text{Exp} \left[ -\alpha - \frac{(2-\alpha)}{n} \left( \frac{r_{ph}}{r} \right)^n + \alpha \log \left( \frac{r}{R_b} \right) \right] dt^2 + \left( 1 + 2 \left( \frac{r_{ph}}{r} \right)^n + \alpha \left( 1 - \left( \frac{r_{ph}}{r} \right)^n \right) \right) dr^2 + r^2 d\Omega^2. \quad (33)$$

Note that Eq. (33) represents a class of spacetimes that depend on the parameter  $n$ . One can also select a different ansatz for the effective potential and obtain another class of spacetimes.

### A. Causal structure of the proposed dark matter spacetime and energy conditions

From the expressions of the Kretschmann scalar ( $R_{\alpha\beta\gamma\delta}R^{\alpha\beta\gamma\delta}$ ) and Ricci scalar, it can be seen that both the scalars diverge at  $r = 0$ , which implies the existence spacetime singularity at the center.

To have an event horizon in a static spacetime, the following condition must be followed at the event horizon radius ( $r_e$ ):

$$\lim_{r \rightarrow r_e} \frac{dt}{dr} = \pm \sqrt{\frac{g_{rr}}{g_{tt}}} = \pm \infty. \quad (34)$$

One can check that, in the proposed dark matter spacetime [Eq. (33)], the above condition is satisfied only for  $r_e = 0$ . This implies that the spacetime does not have any event horizon covering the singularity. On the contrary, the singularity itself is a null singular point. Therefore, the singularity is visible to the outside observer at future timelike infinity ( $I^+$ ).

Nevertheless, in order to be a physically valid solution of Einstein's field equations, the dark matter spacetime should satisfy the weak energy conditions. Using Einstein's field equations, we can compute the energy density and pressures of dark matter spacetime as

$$\rho = \frac{\alpha(1+\alpha) + \beta(1-n+2\alpha)(2-\alpha) + \beta^2(2-\alpha)^2}{\kappa r^2(1+\alpha + \beta(2-\alpha))^2}, \quad (35)$$

$$P_r = 0, \quad (36)$$

$$P_\theta = P_\phi = \frac{1}{4}(\alpha + \beta(2-\alpha))\rho. \quad (37)$$

In Fig. 1, the permitted region (i.e., the shaded region) for which weak energy conditions are fulfilled is depicted in the space of  $n$  and  $r$ . One can observe that the weak energy conditions are satisfied for  $n \leq 1$  and violated for  $n > 1$ . Therefore, throughout the paper, we consider the value of parameter  $n = 1$ .

The causal nature of the singularity can be ascertained by studying the Penrose diagram of spacetime. In a Penrose diagram, the temporal and radial coordinates of the metric are transformed in such a way that the entire spacetime manifold can be adequately represented in a finite-sized causal diagram. In Fig. 2, we show the Penrose diagram of the dark matter spacetime for  $n = 1$ . From the figure, it can be concluded that the singularity at  $r = 0$  in spacetime (33) is null-like in nature.

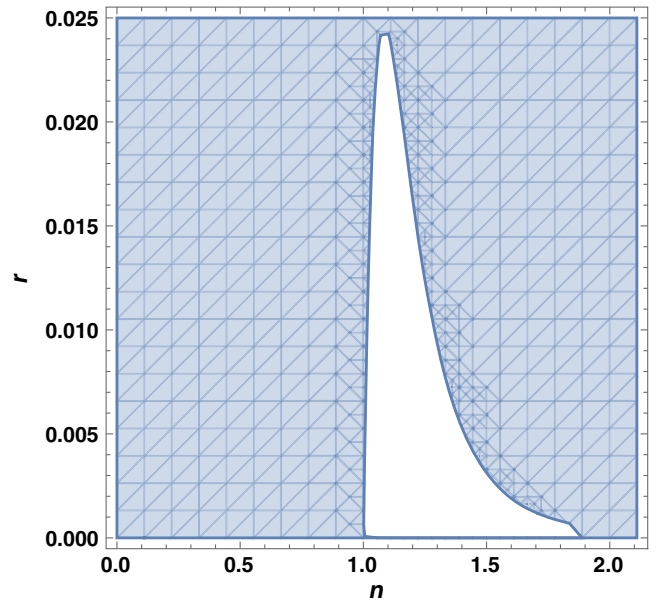


FIG. 1. Figure shows range of weak energy condition violation (i.e., white region). Therefore, the condition  $\rho + P_r > 0$  is satisfied for any value of  $r$  when  $n \leq 1$ .

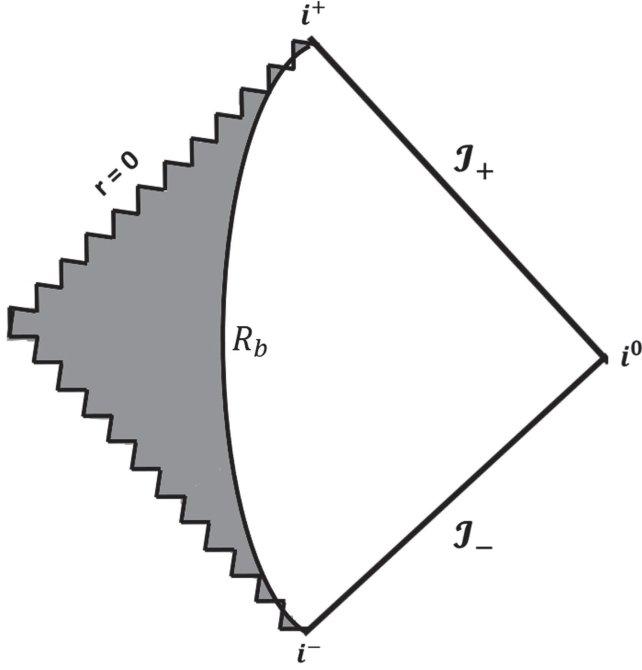


FIG. 2. Carter-Penrose diagram of the dark matter spacetime written in Eq. (33) for  $n = 1$ . The null-like singularity at  $r = 0$  is shown by black zigzag lines. The corresponding future null infinity ( $\mathcal{J}_+$ ), past null infinity ( $\mathcal{J}_-$ ), past timelike infinity ( $i^-$ ), future timelike infinity ( $i^+$ ), and spacelike infinity ( $i^0$ ) are shown. Here  $R_b$  is matching radius with constant radial distance. Gray color shows the interior dark matter spacetime.

From the next section onward, we shift our attention to the observational aspects of our proposed dark matter spacetime with a null-like singularity at the Galactic Center.

### III. OBSERVATIONAL CONSTRAINTS ON DARK MATTER SPACETIME FROM THE ORBITAL DYNAMICS OF THE S2 STAR

Before going into the orbital dynamics of the S2 star and the corresponding observational constraints on dark matter spacetime, in the next subsection, we derive the orbit equation of a test particle freely falling in a spherically symmetric and static spacetime [Eq. (1)].

#### A. Timelike geodesics in dark matter spacetime

In this subsection, we study the timelike bound orbit of the test particle in the static and spherically symmetric spacetime given by Eq. (33).

For bound orbits, the total energy of the particle is greater than or equal to the minimum of the effective potential, i.e.,  $E \geq V_{\min}$ . For the minimum of the effective potential, the following condition should be obeyed:

$$\frac{dV_{\text{eff}}}{dr} = 0, \quad \left. \frac{d^2V_{\text{eff}}}{dr^2} \right|_{r_s} > 0, \quad (38)$$

where  $r = r_s$  is the radius at which  $V_{\text{eff}}(r)$  has a minimum value and the stable circular orbit of a massive particle exists. Here, the  $V_{\text{eff}}(r)$  is given by Eq. (7). The bound elliptical orbits of the particle exist for  $V_{\text{eff}} < E < 0$ . For the bound orbit, the periapsis ( $r_{\min}$ ) and apoapsis ( $r_{\max}$ ) of the orbit can be calculated using the condition  $V_{\text{eff}} - E = 0$ . Therefore, one can define the bound orbits of the freely falling particles in the following way:

$$\begin{aligned} V_{\text{eff}}(r_{\min}) = V_{\text{eff}}(r_{\max}) &= E, \\ E - V_{\text{eff}}(r) &> 0, \quad \forall r \in (r_{\min}, r_{\max}). \end{aligned} \quad (39)$$

For some given conserved values of  $h$  and  $E$ , the shape of the timelike orbit can be determined by describing how the radial coordinate  $r$  changes with the azimuthal coordinate  $\phi$ . Using Eq. (6) and the metric in Eq. (1), we can write

$$\frac{d\phi}{dr} = \frac{h}{r^2} \frac{\sqrt{g_{rr}(r)g_{tt}(r)}}{\sqrt{2(E - V_{\text{eff}})}}. \quad (40)$$

Using the above equation, the orbit equation for a static and spherically symmetric spacetime can be written as

$$\begin{aligned} \frac{d^2u}{d\phi^2} + \frac{u}{g_{rr}(u)} - \left[ \frac{u^2}{2g_{rr}^2(u)} + \frac{c^2}{2g_{rr}^2(u)h^2} - \frac{e^2}{2g_{tt}(u)g_{rr}^2(u)h^2} \right] \\ \times \frac{dg_{rr}(u)}{du} + \frac{e^2}{2g_{tt}^2(u)g_{rr}(u)h^2} \frac{dg_{tt}(u)}{du} = 0, \end{aligned} \quad (41)$$

where  $u(\phi) = 1/r$ . We solve the orbit equation numerically to describe the shape of the bound orbit of the test particle in the dark matter spacetime.

#### B. Orbital dynamics

To trace the orbital path of the star, first we have to solve the time-varying geodesic equation, which gives the equations of motion of the test particle,

$$\dot{t} = \sqrt{\frac{E}{c^2 g_{tt}^2 r(\tau)}}, \quad (42)$$

$$\ddot{r} = \frac{1}{2g_{rr}(r(\tau))} \left[ -c^2 \frac{dg_{tt}(r(\tau))}{dr} \dot{t}^2 - \frac{dg_{rr}(r(\tau))}{dr} \dot{r}^2 + 2r\dot{\phi}^2 \right], \quad (43)$$

$$\dot{\phi} = \frac{h}{r(\tau)^2}. \quad (44)$$

The numerical solutions of Eq. (43) provide the orbital positions over the time.

In terms of the Cartesian coordinates, we express the position and velocity of a particle moving along a real orbit as  $(x, y, z)$  and  $(v_x, v_y, v_z)$ , respectively. For the  $\theta = \pi/2$

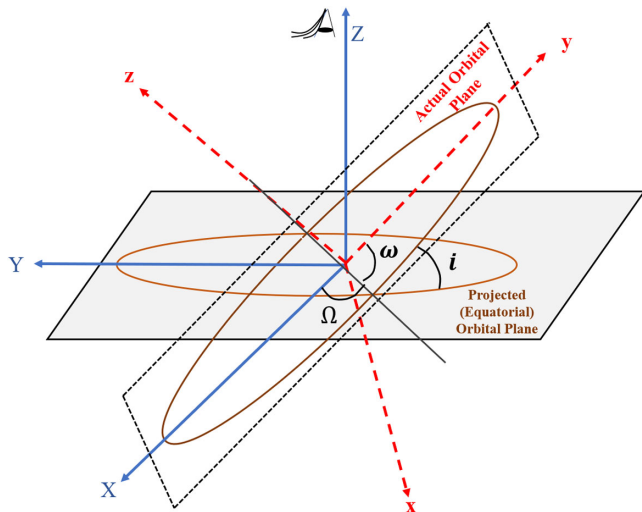


FIG. 3. This figure shows a projection of the actual orbital plane onto the projected orbital plane seen by the asymptotic observer. The focus of the ellipse gives the location of the Sgr A\* compact object. Here, the Z axis of the coordinate system is defined by the vector pointing from the Galactic Center to the Solar System.

case, these can be obtained by transforming the coordinates from spherical Schwarzschild to Cartesian:

$$x = r \cos \phi, \quad y = r \sin \phi, \quad z = 0. \quad (45)$$

The solution of the orbit equation [Eq. (43)] allows us to trace the stellar position, but in order to compare it to observational data, we must first establish the relation between the real orbit and the apparent orbit in the observer's sky. We use classic Thiele-Innes constants, which are  $A$ ,  $B$ ,  $C$ ,  $F$ ,  $G$ , and  $H$ , to obtain the theoretical apparent orbit on the plane of sky given by coordinates  $(X, Y, Z)$  from the real orbit coordinates  $(x, y, z)$  [see Fig. 3],

$$X = xB + yG, \quad (46)$$

$$Y = xA + yF, \quad (47)$$

$$Z = xC + yH, \quad (48)$$

where

$$A = \cos \Omega \cos \omega - \sin \Omega \sin \omega \cos i, \quad (49)$$

$$B = \sin \Omega \cos \omega + \cos \Omega \sin \omega \cos i, \quad (50)$$

$$C = \sin \omega \sin i, \quad (51)$$

$$F = -\cos \Omega \sin \omega - \sin \Omega \cos \omega \cos i, \quad (52)$$

$$G = -\sin \Omega \sin \omega + \cos \Omega \cos \omega \cos i, \quad (53)$$

$$H = \cos \omega \sin i, \quad (54)$$

where  $\omega$ ,  $i$ , and  $\Omega$  are the argument of the pericenter, the inclination between the real orbit and the observation plane, and the ascending node angle, respectively.

General relativity predicts that a star orbiting close to a supermassive compact object is supposed to experience a relativistic redshift. A total redshift  $[z(r)]$  is a combination of the special relativistic Doppler shift and the gravitational redshift. The redshift function can be written as [78]

$$z = \gamma - 1 + u_Z, \quad (55)$$

where

$$u_Z = (\dot{r} \sin(\phi + \omega) + r \dot{\phi} \cos(\phi + \omega)) \sin i \quad (56)$$

is the apparent four-velocity of the emitter, and  $\gamma = \frac{dt}{d\tau} = \frac{\sqrt{E}}{c g_{tt}}$  is the Lorentz factor. In the weak field limit,  $\gamma \rightarrow 1$ . Therefore, the redshift is given by the Keplerian (Newtonian) contribution ( $z_K$ ), where

$$z_K \equiv u_Z. \quad (57)$$

Here we consider the gravitational constant ( $G$ ) and the velocity of light ( $c$ ) as  $4.30091 \times 10^{-3} \text{ pc} M_\odot (\text{km/s})^2$  and  $3 \times 10^8 \text{ km/s}$ , respectively. Using these universal constants, we get the radial distance in the parsec unit.

### C. Orbit of the S2 star around Sgr A\*

The motions of the S stars that comprise the nuclear cluster at the center of the Milky Way have been closely monitored for over three decades. Their trajectories revealed the presence of a supermassive compact object with a mass of  $4 \times 10^6 M_\odot$  at the cluster center. The most important S-cluster member is S2, which has an orbital period of about 16 years around Sgr A\*. It made its closest approach in May 2018, at a distance of 120 A.U. from Sgr A\* with a velocity of 2.7% of the speed of light. This close proximity of S2 to the Sgr A\* compact object causes the relativistic redshift, which is the combination of the transverse Doppler shift from special relativity and the gravitational redshift from general relativity. Here, we use the astrometric data of the S2 star, which were obtained using speckle imaging with a near-infrared camera on Keck I (1995–2005) and adaptive optics imaging with near-infrared camera 2 on Keck II (2005–2018) [50]. In this paper, we use the data of the astrometric positions of S2 given in the supplementary material of [50]. Here, we want to determine the values of the free parameters of the theory from the astrometric data of the S2 star. Comparative differences between observational and theoretical data for dark matter spacetime are given in Fig. 4.

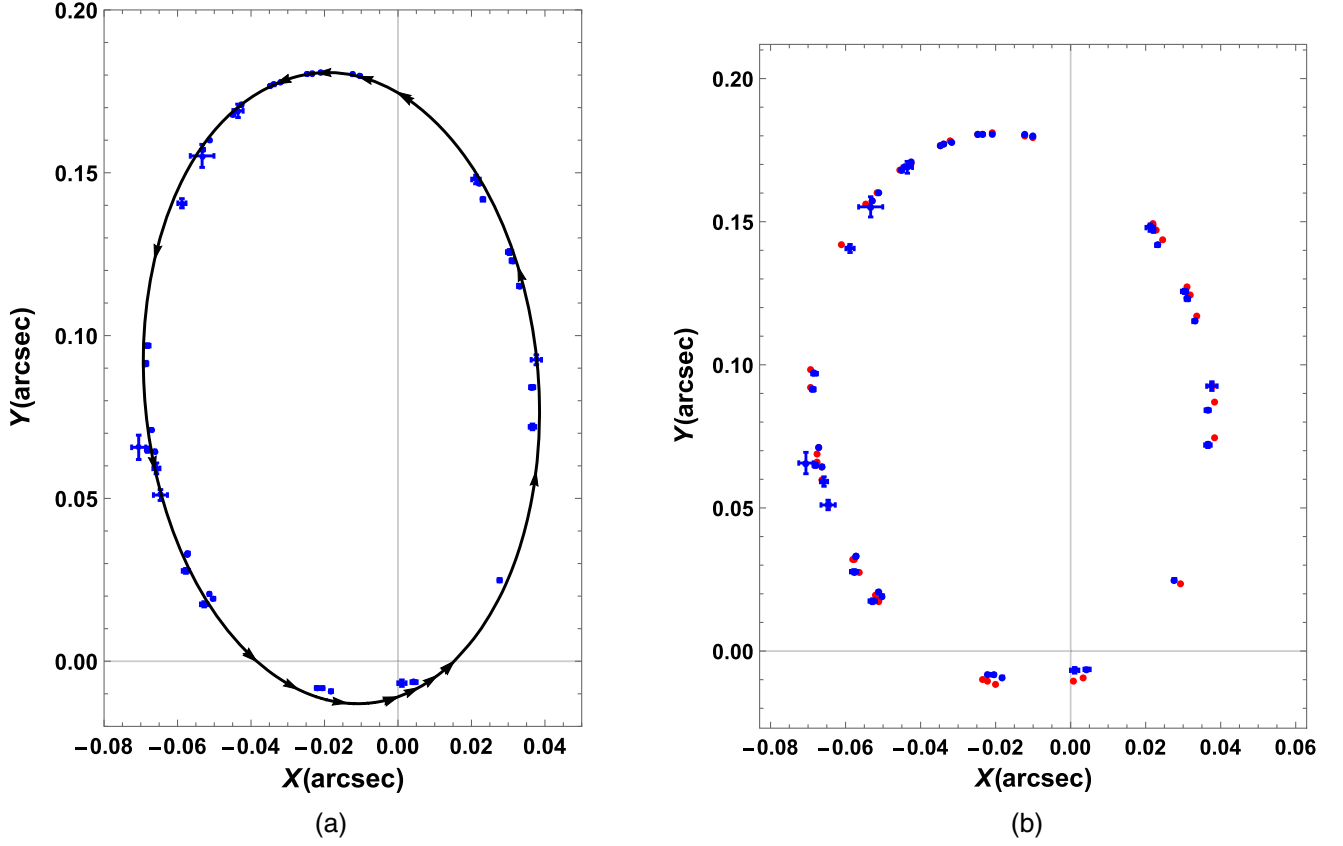


FIG. 4. Theoretical and observed orbits of the S2 star around Sgr A\*. In (a), blue crosses correspond to the original data of the S2 star, and the black curve represents the best-fit dark matter spacetime timelike orbit with the orbital data. (b) Represents the comparison between the experimental data points and the theoretically fitted data points. Here, the theoretical orbit is calculated by solving the equations of motion of a test particle in dark matter spacetime. We use the observational data given in [50].

#### D. Parameter estimation from orbital dynamics

In the present paper, we have used the Metropolis-Hastings Monte Carlo Markov Chain algorithm (MH-MCMC) to find the best-fit values of parameters to the astrometric data of the S2 star [79,80]. Let us consider a parameter  $\psi$  which is random with normal distribution  $\pi(\psi)$ , where  $\pi(\psi)$  is prior distribution that gives us prior uncertainty regarding  $\psi$ . To estimate best-fit parameters using the posterior analysis with some data ( $\mathcal{D}$ ), that is, using the Bayesian inference,

$$\pi(\psi|\mathcal{D}) = \frac{\pi(\psi)p(\mathcal{D}|\psi)}{p(\mathcal{D})} \propto \pi(\psi)p(\mathcal{D}|\psi), \quad (58)$$

where  $\pi(\psi)$  is the prior,  $p(\mathcal{D}|\psi)$  is the likelihood, and  $p(\mathcal{D})$  is marginal probability density function (PDF) of  $\mathcal{D}$ ,

$$p(\mathcal{D}) = \int_{\psi} \pi(\psi)p(\mathcal{D}|\psi)d\psi, \quad (59)$$

which can be regarded as a normalizing constant as it is independent of  $\psi$ . The posterior PDF is thus proportional to the product of prior and likelihood.

#### 1. Priors

In the model, we considered ten free parameters. The prior distribution  $[\pi(\psi)]$  is normally distributed over parameter  $\psi$  with an initial value  $\mu$  and dispersion  $\sigma$ ,  $\mathcal{N}(\mu, \sigma)$ . Here, we adopt six informative initial values of parameters from the previous paper [78] and four noninformative initial values. The distances from Earth to the Galactic Center ( $R_0$ ), argument of the pericenter ( $\omega$ ), inclination ( $i$ ), and ascending node ( $\Omega$ ) are 8190 pc,  $66.4^\circ$ ,  $134.3^\circ$ , and  $227.9^\circ$ , respectively, which are directly taken from the paper [78]. While using the semimajor axis ( $a$ ) (0.1252 arcsec) and eccentricity ( $\epsilon$ ) (0.88), we have calculated the distance to the pericenter and apocenter, using  $r_{\min} = a(1 - \epsilon)$  and  $r_{\max} = a(1 + \epsilon)$ , respectively.

For the two known turning points of the orbit, which are  $r_{\min}$  and  $r_{\max}$ , we can obtain angular momentum ( $h_c$ ) and energy ( $E_c$ ) at the turning points using Eq. (39),

$$h_c = \sqrt{\frac{c^2 r_{\min}^2 r_{\max}^2 (g_U(r_{\min}) - g_U(r_{\max}))}{(r_{\min}^2 g_U(r_{\max}) - r_{\max}^2 g_U(r_{\min}))}}, \quad (60)$$

$$E_c = g_{tt}(r_{\min}) \left( c^2 + \frac{h_c^2}{r_{\min}^2} \right). \quad (61)$$

For noninformative initial values, that is, matching radius ( $R_b$ ), flat velocity at matching radius ( $V_b$ ), radius of photon sphere ( $r_{ph}$ ), and initial time, we consider intuitive values with the previous observation, which are 8190 pc, 150 km/s,  $3GM/c^2$ , and 1 yr, respectively.

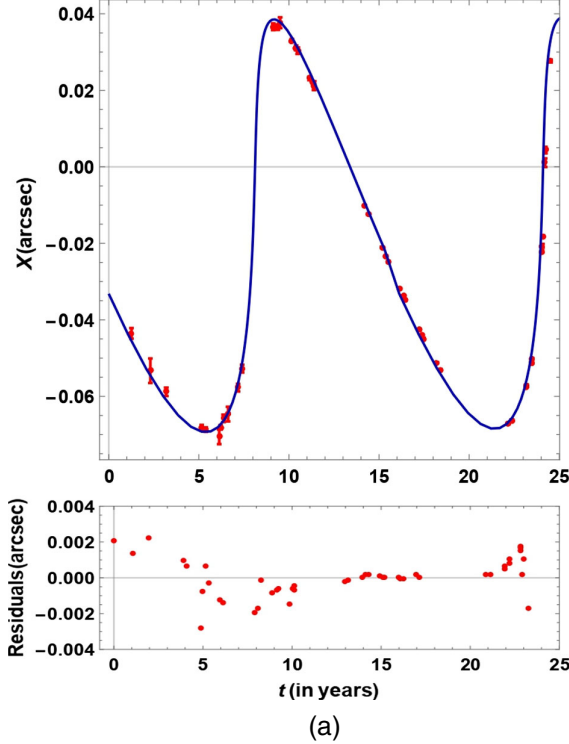
Using the above values, we can numerically integrate the equations of motion (42)–(44) giving appropriate initial conditions at the initial proper time. Once the initial conditions are established, the coordinates of the orbit of S2 at any time  $t$  can be predicted.

## 2. Likelihood

In order to calculate the goodness of fit, we compute the reduced  $\chi^2$  value for each of the observables. The likelihood function [ $p(\mathcal{D}|\psi)$ ] is used in the MH-MCMC analysis with some symmetric error,

$$-\log \mathcal{L} \propto \sum_i \left[ \left( \frac{X_{e,i} - X_i}{\sigma_i^X} \right)^2 + \left( \frac{Y_{e,i} - Y_i}{\sigma_i^Y} \right)^2 \right], \quad (62)$$

where  $(X_e, Y_e)$  are the observed astrometric data and  $(\rho_X, \rho_Y)$  are the error values in the observed data.  $X$  and  $Y$  are theoretical calculated values of trajectories of the S2 star.



## 3. $\chi^2$ analysis

We do not sample the posterior distribution of the model, but rather a minimum  $\chi^2$  value. For numerical  $\chi^2$  computation, we have taken 300000 data points from the normal distribution to calculate the minimum  $\chi^2$  value. We ran six chains for 50000 steps and discovered that the stationarity of data converged to the lowest  $\chi^2$  value around 5.92 for the astrometric data of the S2 star. In our computational chain, the initial  $\chi_i^2$  is greater than the final  $\chi_f^2$ . Therefore, if  $e^{(\chi_i^2 - \chi_f^2)} > 1$ , we accept the jump; if not, it is rejected.

From the observer plane, we fit  $(X, Y)$  [see in Figs. 5(a) and 5(b) with residuals]. We also fit the redshift factor  $Z(r)$ , as shown in Fig. 6. Here, the total  $\chi^2$  value can be taken as the average of the two,

$$\langle \chi^2 \rangle \equiv \frac{1}{2} (\bar{\chi}_X^2 + \bar{\chi}_Y^2). \quad (63)$$

All the ten fitted parameter values are tabulated in Table I. By using those parameters, we calculate the mass, eccentricity, and distance to the pericenter and apocenter. We have also investigated the precession angle, which is 21.6 arc min per orbital period. The best-fit value of  $r_{ph}$  provides information about the shadow size. As we have now determined the best-fit values of the parameters for the

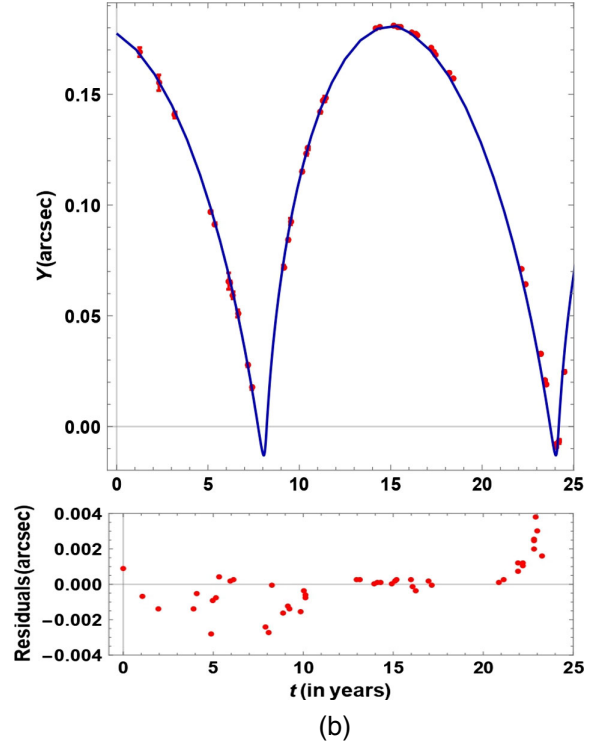


FIG. 5. Plot of  $X$  and  $Y$  as a function of time, along with the respective residuals of the best fit for the dark matter spacetime. In (a) and (b), red crosses correspond to the original data of the S2 star, and the blue curves represent the best fit of the theoretical prediction of dark matter spacetime.

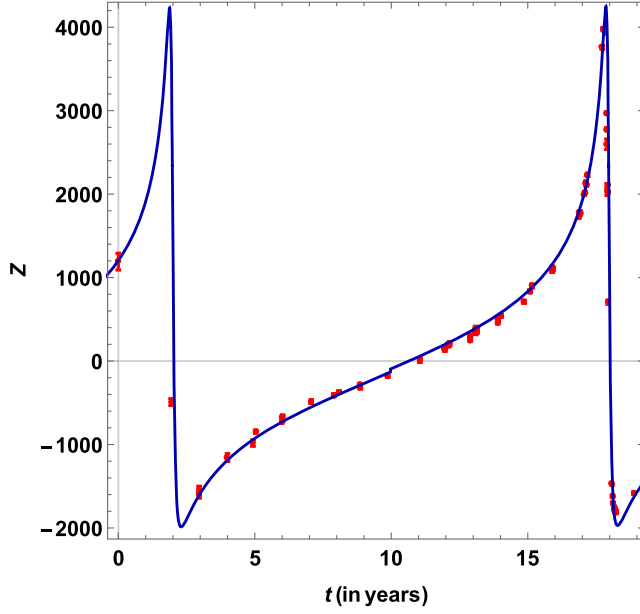


FIG. 6. Figure shows the fitting of redshift data with dark matter spacetime. The blue line represents theoretical fitting, while the red dot represents experimental data. The observational data are taken from [50].

Milky Way Galaxy, we move forward to analyze the redshift, rotation profile, and shadow property of the dark matter spacetime using those best-fit values.

Figure 6 shows the redshift function  $z$  for the dark matter model for the S2 star orbit. The theoretical redshift function

TABLE I. Summary of best-fit values of the model and the orbital parameters for S2 within the dark matter model.

Parameter	Dark matter spacetime
Total mass of sark matter, $M \odot$	$3.947 * 10^{12}$
Distance to pericenter (arcsec)	0.000552
Distance to apocenter (arcsec)	0.009665
Eccentricity	0.89194
$h$ , pc(km/s)	4.4499392
$E$ , $(\text{km/s})^2$	$8.99956211840861 * 10^{10}$
$R_b$ , parsec(pc)	976693
$V_b$ , km/s	131.826
$r_{ph}$ , pc	$2.10256 * 10^{-7}$
Argument of pericenter, $\omega$ ( $^\circ$ )	68.6008
Inclination, $i$ ( $^\circ$ )	133.902
Ascending node, $\Omega$ ( $^\circ$ )	229.935
$R_0$ , pc	8196.4033
Initial time, yr	1.2619854
Orbital period, $P$ (yr)	16.2553
Shadow size (pc)	$5.71538 * 10^{-7}$
Precession angle (arc min)	21.6'
$\bar{\chi}_X^2$	3.92665
$\bar{\chi}_Y^2$	7.91589
$\langle \bar{\chi}^2 \rangle$	5.92127

$z$  is computed using Eq. (55) by taking into account the best-fit values of parameters shown in Table I.

#### IV. GALACTIC ROTATION CURVE

The rotational velocity of the particle in the dark matter spacetime can be obtained by substituting  $g_{tt}(r)$  from Eq. (31) in Eq. (19),

$$V_c = \sqrt{\frac{V_b^2(r - r_{ph}) + c^2 r_{ph}}{r}}, \quad (64)$$

where  $V_b = \sqrt{\frac{GM}{R_b}}$ . Here,  $G$ ,  $R_b$ , and  $M$  are the gravitational constant, halo radius, and total mass of the galaxy enclosed in the halo radius, respectively. Here, the circular velocity profile changes with the radial distance. From Eq. (64), one can see that the circular velocity  $V_c = V_b$  near  $r = R_b$  where  $R_b \gg r_{ph}$ . For the velocity profile of the Milky Way Galaxy, here we use the data provided in Ref. [81]. Figure 7(a) shows the fitting of the theoretical rotation curve with the observations of the Milky Way Galaxy. In Fig. 7(a), the red crosses correspond to the rotational velocity data of our Milky Way Galaxy [81], and the blue line shows the theoretical circular velocity of the test particle calculated from Eq. (64) using the best-fit parameters. The black dotted vertical line at  $r = 976$  kpc represents the boundary of dark matter (DM) spacetime. We find that the fitting is fairly good, with observations in the region of 20–976 kpc. Therefore, this model of dark matter satisfies the flat rotation curve of the Milky Way far away from the Galactic Center. The full range of data from 1 to 1000 kpc on the logarithmic scale is represented in Fig. 7(b). Our model is unable to explain the rotation curve in the region of 0–0.3 kpc. This is due to our consideration that dark matter dominates over large distances around the halo radius.

#### V. SHADOW OF THE PROPOSED DARK MATTER SPACETIME

The shadow of any spacetime geometry depends upon the nature of the effective potential of the null geodesics in that spacetime. As mentioned in Sec. II, the effective potential for the null geodesics in the equatorial plane is given by Eq. (22). At the turning point of the photon, where  $\dot{r} = 0$  and  $V_{\text{eff}}(r_{tp}) = \frac{1}{b_{tp}^2}$ , we can write the impact parameter ( $b_{tp}$ ) corresponding to the turning point as

$$b_{tp} = \frac{r_{tp}}{\sqrt{g_{tt}(r_{tp})}}. \quad (65)$$

When there exists a maximum value of the effective potential of lightlike geodesics in spacetime, and that maximum value is also the upper bound of the potential,

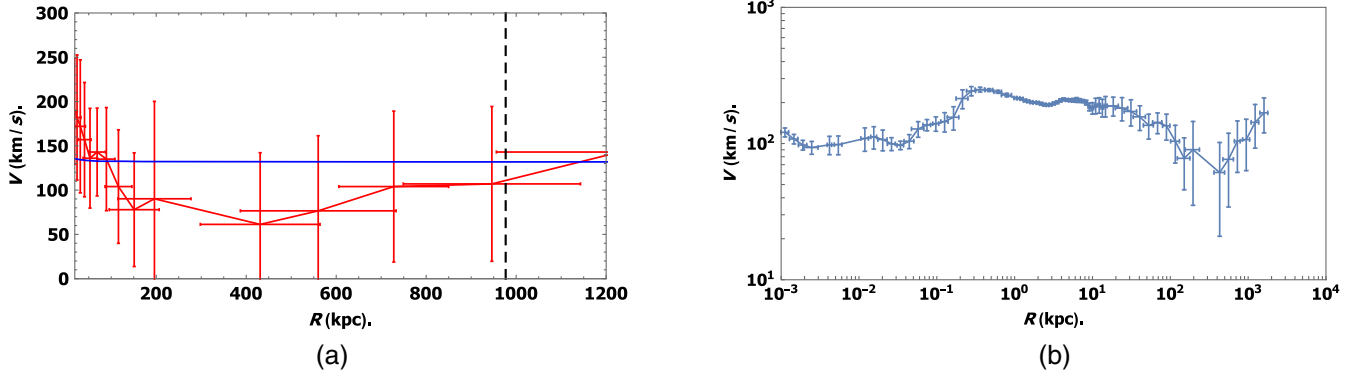


FIG. 7. Rotation curve of the Milky Way Galaxy. The red crosses in (a) correspond to the original data of a flat velocity curve, and the blue line represents the best-fit velocity curve in the range of 20–976.6 kpc. The black dotted line represents the estimated boundary of the halo radius. (b) Represents the logarithmic plot between the experimental data of the velocity of stars with radial distance.

the minimum impact parameter of a photon is the impact parameter associated with the photon sphere ( $b_{ph}$ ). This minimum impact parameter is the critical impact parameter ( $b_{crit} = b_{ph}$ ), which differentiates photons colliding with the central object from those reaching a minimum distance and returning to infinity. Photons from a remote source with an impact parameter  $b$  greater than the critical impact parameter  $b_{ph}$  are scattered and reach the observer. On the other hand, photons with impact parameters less than the critical impact parameter are trapped inside the photon sphere and never reach the observer, resulting in a dark area or shadow in the observer's sky. Therefore, the shadow in the observer's sky appears to be a circular two-dimensional dark disk with a radius of  $b_{crit}$ .

As we know, the shadow of a massive object forms due to the accreting matter surrounding it. Therefore, we need to compute the intensity of light emitted by the accreting matter to obtain the shadow of the massive object in the observer's sky. In order to get the intensity map of the emitting area, we need to consider various radiating processes and emission mechanisms. The measured intensity at the observer's sky point ( $X, Y$ ) can be given as [82]

$$I_{\nu_{obs}}(X, Y) = \int_{\gamma} g^3 j(\nu_e) dl_{prop}, \quad (66)$$

where  $g = \nu_{obs}/\nu_e$  is the redshift factor,  $\nu_{obs}$  is the observed photon frequency,  $\nu_e$  is the photon frequency as measured in the rest frame of the accreting gas that is emitting radiation,  $j(\nu_e)$  is the emissivity per unit volume in the rest frame of the emitter, and  $dl_{prop} = k_{\alpha} u_e^{\alpha} d\lambda$  is the infinitesimal proper length in the rest frame of the emitter. The integration is done along the photon path ( $\gamma$ ). The redshift factor can be given by [82]

$$g = \frac{k_{\alpha} u_{obs}^{\alpha}}{k_{\beta} u_e^{\beta}}, \quad (67)$$

where  $u_{obs}^{\alpha} = (1, 0, 0, 0)$  is the four-velocity of the distant static observer,  $u_e^{\beta}$  is the timelike four-velocity of the emitter,  $\lambda$  is the affine parameter, and  $k_{\alpha}$  is the four-velocity of the photon. For simplicity, here we consider a simple model of spherically symmetric accreting gas that is freely falling radially and it is optically thin (i.e., the accreting matter does not absorb photons). In a generic, spherically symmetric, static spacetime (1), the components of the four-velocity of a radially freely falling particle can be evaluated as

$$u_e^t = \frac{1}{g_{tt}}, \quad u_e^r = -\sqrt{\frac{(1-g_{tt})}{g_{tt}g_{rr}}}, \quad u_e^{\theta} = u_e^{\phi} = 0. \quad (68)$$

Using Eq. (68), the redshift factor can be written as

$$g = \frac{1}{\frac{1}{g_{tt}} - \frac{k_r}{k_t} \sqrt{\frac{(1-g_{tt})}{g_{tt}g_{rr}}}}, \quad (69)$$

where

$$\frac{k^r}{k^t} = \sqrt{\frac{g_{tt}}{g_{rr}} \left(1 - \frac{g_{tt} b^2}{r^2}\right)}. \quad (70)$$

In the present work, we assume a simple model for the specific emissivity in which the radiation from emitter is monochromatic with the emitter's rest frame frequency  $\nu_*$  and radially falls by  $1/r^2$ ,

$$j(\nu_e) \propto \frac{\delta(\nu_e - \nu_*)}{r^2}, \quad (71)$$

where  $\delta$  is the Dirac  $\delta$  function. Now, Eq. (72) can be written as [82]

$$I_{obs}(X, Y) \propto - \int_{\gamma} \frac{g^3 k_t dr}{r^2 k^r}, \quad (72)$$

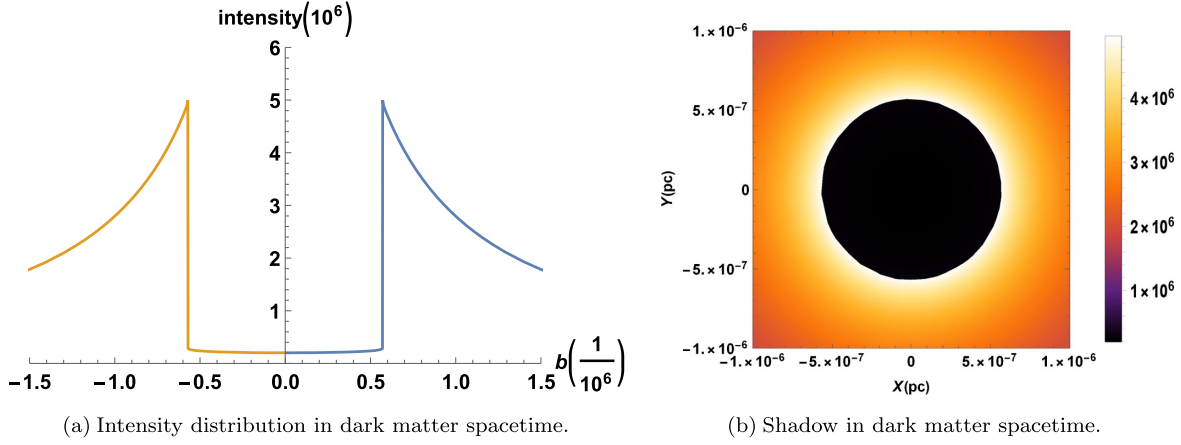


FIG. 8. In this figure, the intensity map in the observer’s sky (a) and the shadow of the central object (b) are shown for dark matter spacetime. The radius of the shadow of dark matter spacetime (b) is  $5.7154 \times 10^{-7}$  pc.

where  $I_{\text{obs}}(X, Y)$  denotes the intensity distribution in the  $(X, Y)$  plane of the observer’s sky and  $X^2 + Y^2 = b^2$ . Now, using the above Eq. (72), we can simulate the shadow.

We employed a technique called “backward ray tracing” to simulate the shadow, which involves tracing light rays backward in time from the observer to the source.

Using the best-fitting parameters, we construct the shadow of Sgr A\* using the dark matter model, which is presented in Fig. 8. The radius of the shadow is found to be  $5.7154 \times 10^{-7}$  pc.

### A. Limitation and constraints in the paper

- (i) Here we assume that the S2 star moves in the gravitational potential of a single central compact object with an Arnowitt-Deser-Misner mass  $M$ . Therefore, the gravitational effect of the other object inside the S2 is neglected, like the G2 object.
- (ii) In this paper, we do not consider radio source data. Hence, we are not able to best fit the observed location of the central radio source for Sgr A\*, which may confirm the center of our Milky Way Galaxy. However, the best-fit theoretical prediction of the centroid of mass yields reasonable results that match the existing data.
- (iii) Here, data are fitted with only the astrometric position of the S2 star. We have not used spectroscopic data in the fitting procedure.
- (iv) The orbital region of an S2 star is considered in the weak gravitational field in order to use the Thiele-Innes constants. We have neglected the Shapiro time delay, which differs no more than 5–6 min in the orbital period of the S2 star.

## VI. DARK MATTER DISTRIBUTION AND OBSERVATIONAL IMPLICATION

A considerable amount of research has been dedicated to studying dark matter profiles in the Milky Way Galaxy,

with a specific focus on understanding various regions of our Galaxy. In our Universe, dark matter typically constitutes the dominant component of galaxies. The prediction of the spacetime geometry for the dark matter distribution is a challenging task. However, in this paper, we endeavor to model the global picture of the dark matter distribution in galaxies within the framework of the general theory of relativity.

There are works that explain the effect of dark matter on shadows and trajectories. In [70], the investigation is on whether current and future astronomical observations of Sgr A\* could detect the presence of such a DM spike. In their study, they made an assumption regarding the distribution of dark matter between  $R_{sp}$  and  $r_b$ , where  $r_b$  represents the inner edge of the DM spike. The DM mass shell they considered is essentially a fixed mass influenced by its position and density. However, they overlooked the impact of the external matching metric, which can be matched with either the Burkert-Salucci profile or the NFW dark matter profile. Consequently, their presentation displays the distribution of dark matter in fragmented parts, lacking a comprehensive single profile that incorporates the galaxy’s metric within the context of general relativity.

Our primary motivation is to demonstrate a broad formalism for which we can demonstrate the complete galactic metric with a central singularity [not the dark matter distribution at the Sgr A\* compact object (near the spike)]. Due to the spread of dark matter, central compact objects may alternatively be a null singularity rather than a black hole. The role of central singularity in galaxy formation is an intriguing topic. In the context of the general theory of relativity, this type of information provides the primordial structure of the galaxy.

Our fitting parameters for the globally structured DM spacetime offer valuable insights into the total distributed dark matter within the galactic radius  $R_b$ . The Milky Way Galaxy’s total mass and boundary radius are

$3.947 \times 10^{12} M_{\odot}$  and 976,693 pc, respectively. In this paper, our primary motivation is to develop a metric that not only exhibits a flat velocity curve but also incorporates a shadow within the distribution of dark matter in the range  $0 < r < R_b$ . Specifically, for  $r \sim R_b$ , we consider the Newtonian metric, representing a weak gravitational field region of the Schwarzschild metric. The best-fit parameters we obtained suggest that the central singularity might be a null singularity rather than a black hole. Throughout our study, we extensively explored several key topics, including the possible geometric structures of a galaxy, the existing astrometric data of the S2 star, the shadow size of the central compact body Sgr A\*, and the data of the galactic rotation curve. By incorporating all these key properties of a galaxy, we derived a class of spacetime metrics that encapsulates these important features.

The EHT Collaboration recently unveiled an image of the central compact object in our Milky Way Galaxy (Sgr A\*). This image revealed an estimated angular shadow with a diameter of  $48.7 \pm 7 \mu$  arcsec [20,83]. In our article, we employ a different approach, estimating the shadow's size to be approximately  $28.8 \pm 9 \mu$  arcsec based on the best-fit data obtained from the galactic rotation curve and astrometric data derived from the S2 star. It is noteworthy that our projected shadow size appears to be smaller than the EHT Collaboration's prediction. It is important to clarify that our results do not claim that the proposed spacetime satisfies all the properties of a galaxy. Instead, we present it as one of the candidates within the class of dark matter spacetime proposed in this article.

## VII. CONCLUSION AND RESULTS

The conclusions from this study can be summarized as follows:

- (i) In this paper, we present a new approach for constructing a viable class of spacetimes for galactic dark matter in the framework of general relativity. We show that one can use the concept of the galactic flat velocity curve and the conditions for the existence of a photon sphere to construct the

$g_{tt}(r)$  metric coefficient. We match the interior dark matter spacetime with the external Schwarzschild spacetime at the matching boundary  $R_b$ . We consider the internal fluid has zero radial pressure ( $P_r = 0$ ) and nonzero tangential pressures ( $P_T$ ). We show that the proposed spacetime satisfies the weak energy conditions and it has a central null singularity.

- (ii) Next, we constrain the free parameters of the metric using the data of the astrometric positions of the S2 star around Sgr A\*. We obtained the orbit equation and solved it numerically, in order to get particle trajectories in the dark matter spacetime, and we compare it with the astrometric data of the S2 star. Using the MCMC algorithm, we obtain the value of photon sphere radius  $r_{ph}$  and constant circular velocity  $V_b$ . The best-fit values derived from the minimum  $\chi^2$  fitting show good agreement with the previously known estimated values, such as the galaxy's mass being around  $3.947 \times 10^{12}$  solar mass, the distance from Earth to the center of the compact object being  $R_0 = 8196$  pc, and the range of the dark matter halo being between 10 and 976.7 kpc, etc.
- (iii) Using the astrophysical best-fit values of the parameters of the proposed dark matter spacetime, we simulate the shadow cast by the same. Additionally, we also plot the redshift function using the best-fit parameter values and fit it with the data.
- (iv) In conclusion, the observed flat rotation curves and the shadow radius can be used to determine the spacetime geometry of the dark-matter-dominated galaxy. Apart from explaining the dynamics of the galaxy away from the galactic center, it can also provide insight into the nature of the compact object present at the galactic center. It should also be noted that we do not claim that the proposed spacetime satisfies all the properties of a galaxy. The proposed spacetime is a simple model of galactic spacetime that is constructed by using some of the important characteristics of a galaxy.

---

[1] M. Persic, P. Salucci, and F. Stel, *Mon. Not. R. Astron. Soc.* **281**, 27 (1996).  
 [2] A. Krut, C. R. Argüelles, J. Rueda, and R. Ruffini, *Astronomy Reports* **62**, 898 (2018).  
 [3] Lars Bergström, *New J. Phys.* **11**, 105006 (2009).  
 [4] M. Milgrom, *Astrophys. J.* **270**, 365 (1983).  
 [5] P. D. Mannheim, *Astrophys. J.* **479**, 659 (1997).  
 [6] M. D. Roberts, *Gen. Relativ. Gravit.* **36**, 2423 (2004).

[7] J. D. Bekenstein, *Phys. Rev. D* **70**, 083509 (2004); **71**, 069901(E) (2005).  
 [8] J. W. Moffat and I. Y. Sokolov, *Phys. Lett. B* **378**, 59 (1996).  
 [9] J. R. Brownstein and J. W. Moffat, *Astrophys. J.* **636**, 721 (2006).  
 [10] M. K. Mak and T. Harko, *Phys. Rev. D* **70**, 024010 (2004).  
 [11] T. Harko and K. S. Cheng, *Astrophys. J.* **636**, 8 (2005).

- [12] C. G. Boehmer and T. Harko, *Classical Quantum Gravity* **24**, 3191 (2007).
- [13] P. S. Joshi and I. H. Dwivedi, *Phys. Rev. D* **47**, 5357 (1993).
- [14] P. S. Joshi, D. Malafarina, and R. Narayan, *Classical Quantum Gravity* **28**, 235018 (2011).
- [15] K. Mosani, D. Dey, and P. S. Joshi, *Phys. Rev. D* **101**, 044052 (2020).
- [16] M. Dafermos and J. Luk, [arXiv:1710.01722](https://arxiv.org/abs/1710.01722).
- [17] K. Bhattacharya, D. Dey, A. Mazumdar, and T. Sarkar, *Phys. Rev. D* **101**, 043005 (2020).
- [18] R. Penrose, *Riv. Nuovo Cimento Soc. Ital. Fis.* **1**, 252 (1969).
- [19] K. Akiyama *et al.* (Event Horizon Telescope Collaboration), *Astrophys. J. Lett.* **875**, L1 (2019).
- [20] K. Akiyama *et al.* (Event Horizon Telescope Collaboration), *Astrophys. J. Lett.* **930**, L12 (2022).
- [21] A. E. Broderick *et al.* (Event Horizon Telescope Collaboration), *Astrophys. J. Lett.* **930**, L21 (2022).
- [22] M. Wielgus *et al.* (Event Horizon Telescope Collaboration), *Astrophys. J. Lett.* **930**, L19 (2022).
- [23] K. Akiyama *et al.* (Event Horizon Telescope Collaboration), *Astrophys. J. Lett.* **930**, L13 (2022).
- [24] K. Akiyama *et al.* (Event Horizon Telescope Collaboration), *Astrophys. J. Lett.* **930**, L14 (2022).
- [25] K. Akiyama *et al.* (Event Horizon Telescope Collaboration), *Astrophys. J. Lett.* **930**, L16 (2022).
- [26] K. Akiyama *et al.* (Event Horizon Telescope Collaboration), *Astrophys. J. Lett.* **930**, L15 (2022).
- [27] J. Farah *et al.* (Event Horizon Telescope Collaboration), *Astrophys. J. Lett.* **930**, L18 (2022).
- [28] K. Akiyama *et al.* (Event Horizon Telescope Collaboration), *Astrophys. J. Lett.* **930**, L17 (2022).
- [29] A. B. Joshi, D. Dey, P. S. Joshi, and P. Bambhaniya, *Phys. Rev. D* **102**, 024022 (2020).
- [30] S. Paul, *Phys. Rev. D* **102**, 064045 (2020).
- [31] D. Dey, R. Shaikh, and P. S. Joshi, *Phys. Rev. D* **102**, 044042 (2020).
- [32] D. Dey, R. Shaikh, and P. S. Joshi, *Phys. Rev. D* **103**, 024015 (2021).
- [33] V. Patel, D. Tahelyani, A. B. Joshi, D. Dey, and P. S. Joshi, *Eur. Phys. J. C* **82**, 798 (2022).
- [34] R. Shaikh, P. Kocherlakota, R. Narayan, and P. S. Joshi, *Mon. Not. R. Astron. Soc.* **482**, 52 (2019).
- [35] D. Tahelyani, A. B. Joshi, D. Dey, and P. S. Joshi, *Phys. Rev. D* **106**, 044036 (2022).
- [36] C. Liu, T. Zhu, and Q. Wu, *Chin. Phys. C* **45**, 015105 (2021).
- [37] C. Liu, S. Yang, Q. Wu, and T. Zhu, *J. Cosmol. Astropart. Phys.* **02** (2022) 034.
- [38] P. S. Joshi, D. Malafarina, and R. Narayan, *Classical Quantum Gravity* **31**, 015002 (2014).
- [39] P. Bambhaniya, S. K. K. Jusufi, and P. S. Joshi, *Phys. Rev. D* **105**, 023021 (2022).
- [40] F. Rahaman, T. Manna, R. Shaikh, S. Aktar, M. Mondal, and B. Samanta, *Nucl. Phys.* **B972**, 115548 (2021).
- [41] T. Harko, Z. Kovacs, and F. S. N. Lobo, *Phys. Rev. D* **78**, 084005 (2008).
- [42] T. Harko, Z. Kovacs, and F. S. N. Lobo, *Phys. Rev. D* **79**, 064001 (2009).
- [43] Z. Kovacs and T. Harko, *Phys. Rev. D* **82**, 124047 (2010).
- [44] T. Harko, Z. Kovacs, and F. S. N. Lobo, *Classical Quantum Gravity* **26**, 215006 (2009).
- [45] J. Q. Guo, P. S. Joshi, R. Narayan, and L. Zhang, *Classical Quantum Gravity* **38**, 035012 (2021).
- [46] A. N. Chowdhury, M. Patil, D. Malafarina, and P. S. Joshi, *Phys. Rev. D* **85**, 104031 (2012).
- [47] R. Abuter *et al.* (GRAVITY Collaboration), *Astron. Astrophys.* **615**, L15 (2018).
- [48] A. Hees, T. Do, A. M. Ghez, G. D. Martinez, S. Naoz, E. E. Becklin, A. Boehle, S. Chappell, D. Chu, A. Dehghanfar *et al.*, *Phys. Rev. Lett.* **118**, 211101 (2017).
- [49] R. Abuter *et al.* (GRAVITY Collaboration), *Astron. Astrophys.* **636**, L5 (2020).
- [50] T. Do, A. Hees, A. Ghez, G. D. Martinez, D. S. Chu, S. Jia, S. Sakai, J. R. Lu, A. K. Gautam, and K. K. O'Neil *et al.*, *Science* **365**, 664 (2019).
- [51] C. Martínez, N. Parra, N. Valdés, and J. Zanelli, *Phys. Rev. D* **100**, 024026 (2019).
- [52] Eva Hackmann and Claus Lämmerzahl, *Phys. Rev. Lett.* **100**, 171101 (2008).
- [53] E. Hackmann, V. Kagramanova, J. Kunz, and C. Lämmerzahl, *Europhys. Lett.* **88**, 30008 (2009).
- [54] Eva Hackmann, Claus Lämmerzahl, Yuri N. Obukhov, Dirk Puetzfeld, and Isabell Schaffer, *Phys. Rev. D* **90**, 064035 (2014).
- [55] I. M. Potashov, J. V. Tchamarina, and A. N. Tsirulev, *Eur. Phys. J. C* **79**, 709 (2019).
- [56] A. B. Joshi, P. Bambhaniya, D. Dey, and P. S. Joshi, [arXiv:1909.08873](https://arxiv.org/abs/1909.08873).
- [57] P. Bambhaniya, A. B. Joshi, D. Dey, and P. S. Joshi, *Phys. Rev. D* **100**, 124020 (2019).
- [58] D. Dey, P. S. Joshi, A. Joshi, and P. Bambhaniya, *Int. J. Mod. Phys. D* **28**, 1930024 (2019).
- [59] P. Bambhaniya, D. N. Solanki, D. Dey, A. B. Joshi, P. S. Joshi, and V. Patel, *Eur. Phys. J. C* **81**, 205 (2021).
- [60] H. Y. Lin and X. M. Deng, *Phys. Dark Universe* **31**, 100745 (2021).
- [61] X. M. Deng, *Phys. Dark Universe* **30**, 100629 (2020).
- [62] X. M. Deng, *Eur. Phys. J. C* **80**, 489 (2020).
- [63] B. Gao and X. M. Deng, *Ann. Phys. (Amsterdam)* **418**, 168194 (2020).
- [64] Daniela Pugliese, Hernando Quevedo, and Remo Ruffini, *Phys. Rev. D* **84**, 044030 (2011).
- [65] P. Bambhaniya, A. B. Joshi, D. Dey, P. S. Joshi, A. Mazumdar, T. Harada, and K. i. Nakao, [arXiv:2209.12610](https://arxiv.org/abs/2209.12610).
- [66] K. Glampedakis and D. Kennefick, *Phys. Rev. D* **66**, 044002 (2002).
- [67] R. Fujita and W. Hikida, *Classical Quantum Gravity* **26**, 135002 (2009).
- [68] D. Pugliese, H. Quevedo, and R. Ruffini, *Phys. Rev. D* **88**, 024042 (2013).
- [69] Prerna Rana and A. Mangalam, *Classical Quantum Gravity* **36**, 045009 (2019).
- [70] S. Nampalliwar, S. Kumar, K. Jusufi, Q. Wu, M. Jamil, and P. Salucci, *Astrophys. J.* **916**, 116 (2021).
- [71] H. Nishikawa, E. D. Kovetz, M. Kamionkowski, and J. Silk, *Phys. Rev. D* **99**, 043533 (2019).
- [72] A. Burkert, *Astrophys. J.* **447**, L25 (1995).
- [73] P. Salucci and A. Burkert, *Astrophys. J. Lett.* **537**, L9 (2000).

- [74] J. F. Navarro, C. S. Frenk, and Simon D. M. White, *Mon. Not. R. Astron. Soc.* **275**, 720 (1995).
- [75] J. B. Hartle, *Gravity—An Introduction to Einstein’s General Relativity* (Pearson Education, Inc., 2003).
- [76] V. C. Rubin, N. Thonnard, and W. K. Ford, Jr., *Astrophys. J.* **238**, 471 (1980).
- [77] E. Poisson, *A Relativist’s Toolkit: The Mathematics of Black-Hole Mechanics* (Cambridge University Press, Cambridge, England, 2009).
- [78] E. A. Becerra-Vergara, C. R. Argüelles, A. Krut, J. A. Rueda, and R. Ruffini, *Astron. Astrophys.* **641**, A34 (2020).
- [79] W. K. Hastings, *Biometrika* **75**, 1 (1970).
- [80] Lorenzo Posti and Amina Helmi, *Astron. Astrophys.* **621**, A56 (2019).
- [81] Y. Sofue, *Publ. Astron. Soc. Jpn.* **65**, 118 (2013).
- [82] C. Bambi, *Phys. Rev. D* **87**, 107501 (2013).
- [83] S. G. Ghosh and M. Afrin, *Astrophys. J.* **944**, 174 (2023).